

# Binding Strength Between Cell Adhesion Proteoglycans Measured by Atomic Force Microscopy

Ulrich Dammer,\* Octavian Popescu,\*† Peter Wagner, Dario Anselmetti, Hans-Joachim Güntherodt, Gradimir N. Misevic‡

Measurement of binding forces intrinsic to adhesion molecules is necessary to assess their contribution to the maintenance of the anatomical integrity of multicellular organisms. Atomic force microscopy was used to measure the binding strength between cell adhesion proteoglycans from a marine sponge. Under physiological conditions, the adhesive force between two cell adhesion molecules was found to be up to 400 piconewtons. Thus a single pair of molecules could hold the weight of 1600 cells. High intermolecular binding forces are likely to form the basis for the integrity of the multicellular sponge organism.

Specific intermolecular recognition is a prerequisite for dynamic biochemical processes in living organisms. Such interactions between biological macromolecules are usually investigated by kinetic binding studies, calorimetric methods, x-ray diffraction, nuclear magnetic resonance, and other spectroscopic analyses. These methods do not provide a direct measurement of the intermolecular binding forces that are fundamental for the function of the ligand-receptor association. Recently, surface force apparatus and atomic force microscopy (AFM) were introduced to quantify the forces of biotin-streptavidin interactions (1–3) or to follow in real time the conformational changes in a single enzyme (4), and optical tweezers were applied to probe the forces responsible for myosin-actin assembly (5). Here, we used AFM to determine the binding strength between cell adhesion macromolecules under various physiological conditions. We selected the cell adhesion proteoglycan (AP) of the marine sponge *Microciona prolifera* as a model. The AP mediates in vivo cell recognition and aggregation via homophilic, specific, polyvalent, and calcium ion-dependent carbohydrate-carbohydrate interactions (6–8).

With the use of AFM imaging, we observed AP rings with a diameter of 200 nm and about 20 irradiating arms, each 180 nm long (Fig. 1A). Although similar structures can be seen by electron microscopy (EM) (Fig. 1B), AFM provides additional three-dimensional information about the ring-arm attachment sites where globular structures are visible.

To measure AP-AP interaction forces, we covalently attached APs to an AFM sensor tip and a flat surface; the attachment process involved AP proteins but did not modify functional carbohydrate adhesion sites (9). The cantilever tip was carefully moved toward the substrate surface, and a series of approach-and-retract cycles was collected (10). The stability of binding events during the course of these experiments indicated that none or very few of the AP functional adhesion sites were irreversibly damaged. Four typical approach-and-retract cycles originating from AP experiments are shown (Fig. 2, A through D). The adhesion peaks were retarded, indicating that there was no interaction during the surface approach, but on retraction the lever detected an attractive force at a dis-

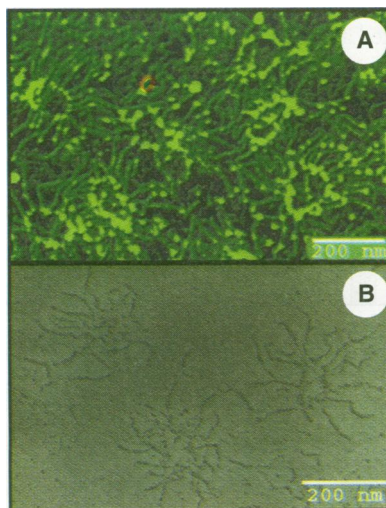


**Fig. 1.** Adhesion proteoglycans imaged by AFM and EM. (A) The APs (16  $\mu\text{g}/\text{ml}$ ) in SWT containing 2 mM  $\text{Ca}^{2+}$  were physisorbed to freshly cleaved mica (15 min), briefly rinsed with nanopure water, and dried in air. AFM images (tapping mode) were taken in air (16). (B) For EM the same procedure as in (A) was used but the mica was charged by APTS (16). After rotary shadowing, APs were imaged by a Hitachi 7000 electron microscope.

tance from 0 to approximately 200 nm above the surface. This phenomenon was also observed within a few nanometers of the surface without actually touching it. In contrast, a typical approach-and-retract cycle taken between two surfaces without APs showed that adhesion took place directly at the surface; this observation indicates the presence of short-range forces, and the slope of the adhesion curve shows that there was no elasticity in the sample itself (Fig. 2E). The shape of the approach-and-retract curves between APs suggests the presence of long-range interactions, interpreted as the lifting and extension of stringlike arms, followed by further stretching until the elastic force of the cantilever equals the strength of the binding and the lever “jumps off.” At a physiological  $\text{Ca}^{2+}$  concentration of 10 mM in seawater tris (SWT) [0.5 M NaCl and 20 mM tris buffer (pH 7.4) iso-osmotic with seawater], multiple jump-offs were frequently observed, indicating polyvalent binding with an average adhesive force of  $40 \pm 15$  pN per release (Fig. 2).

We also characterized AP-AP adhesion

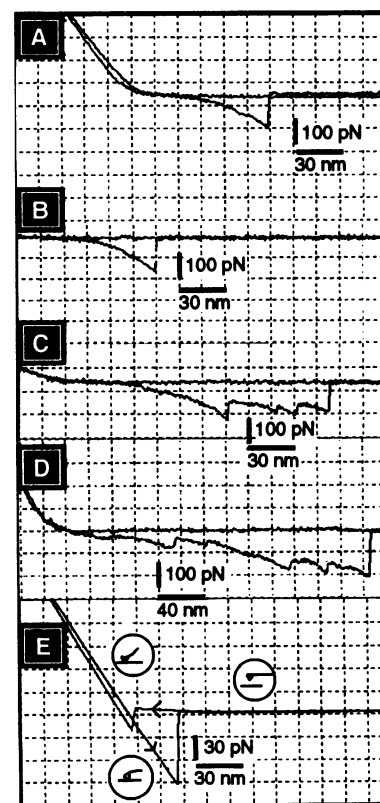


**Fig. 2.** Typical AFM approach-and-retract cycles for AP-AP interactions. The x axis shows the vertical movement of the cantilever; the y axis shows the bending of the cantilever and thus the force acting on it. (A), (B), (C), and (D) represent typical AP-AP interactions, whereas (E) is an example of the interaction between two gold surfaces covered with self-assembled monolayers (1-dodecanethiol).

U. Dammer, D. Anselmetti, H.-J. Güntherodt, Institute of Physics, University of Basel, CH-4056 Basel, Switzerland. O. Popescu and G. N. Misevic, Department of Research, University Hospital of Basel, CH-4031 Basel, Switzerland. P. Wagner, ETH Zürich, Institute of Biochemistry II, CH-8092 Zürich, Switzerland.

\*These authors contributed equally to this study.

†Present address: Institute for Biological Research, 3400 Cluj-Napoca, Romania.

‡To whom correspondence should be addressed.

by measuring both the force necessary to separate the AP-functionalized sensor tip from the AP surface (final jump-offs) and the percentage of interaction events under different ionic conditions (Fig. 3) (11). These two indicators of AP activity varied reversibly with the  $\text{Ca}^{2+}$  concentration, in agreement with AP-promoted cell adhesion (6–8) and AP-coated bead aggregation. At a  $\text{Ca}^{2+}$  concentration of 10 mM, the average force between APs was 125 pN, ranging up to 400 pN, with high probability of binding ( $60 \pm 10\%$ ). At a  $\text{Ca}^{2+}$  concentration of 2 mM, cell adhesion and AP bead aggregation were sharply reduced (6–8), and the force ( $40 \pm 15$  pN) and probability of binding ( $12 \pm 5\%$ ) were also reduced (Fig. 3). The interaction between APs is  $\text{Ca}^{2+}$ -selective, as reported with a cell aggregation assay (12). Indeed, 10 mM  $\text{Mg}^{2+}$  could not replace  $\text{Ca}^{2+}$  in AFM experiments or in adhesion of AP-coated beads (Fig. 3).

Use of the monoclonal antibody (mAb) block 2 provided a third line of evidence that the AFM-measured interactions originate from AP-AP binding. This antibody recognizes a carbohydrate epitope and specifically inhibits AP-promoted cell adhesion (7) and AP-coated bead aggregation (Fig. 3D). In AFM experiments, block 2 Fab fragments in 10 mM  $\text{Ca}^{2+}$  SWT reduced the interactive force to approximately the level measured at 2 mM  $\text{Ca}^{2+}$ . A control mAb did not prevent AP-AP binding under equivalent conditions (Fig. 3C). Thus, during AFM measurements in all tested experimental conditions, AP-AP interactions resemble cell-cell adhesion events observed in vivo.

The shape of the approach-and-retract

cycles shows that stringlike structures were responsible for AP-AP interactions (Fig. 2). These strings are likely to be the AP arms composed of glycans with a relative molecular weight of  $200 \times 10^3$  (g200), which have been shown to mediate polyvalent AP-AP binding (7). This possibility is further supported by the fact that the length (180 nm) (13) and the number (20 copies) of the g200 glycan per AP molecule (7) are similar to the length and number of AP arms as measured by AFM and EM (Fig. 1). Finally, the inhibitory mAb block 2 is directed against a self-association epitope located on the g200 glycan (7).

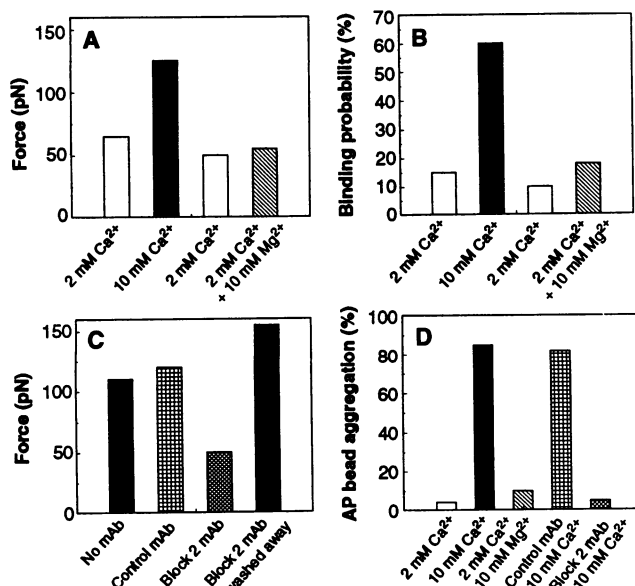
These observations are consistent with a model in which the AP arms are responsible for AP-AP cohesion. Because of their polysaccharide nature, the AP arms did not participate in the AP crosslinking to AFM surfaces and thus remained free to irradiate into the buffer. During each approach-and-retract cycle, multiple noncovalent bonds between arms attached to the sensor tip and arms connected to the substrate were formed and broken. Because the radius of curvature of a typical functionalized AFM tip is about 50 nm and the AP backbone ring is approximately 200 nm in diameter, only a single AP molecule from the tip could participate in the measured interaction with the densely AP-covered surface. The observation that approach-and-retract curves often exhibited multiple jump-off steps (Fig. 2) indicates that binding was polyvalent. Each step of  $40 \pm 15$  pN corresponds to the unbinding of a pair of AP arms, with deviation caused by a varying degree of mutual overlap. The maximal measured adhesion force of 400 pN and the average force of 125 pN are thus interpreted as the binding between 10 and 3 pairs

of AP arms, respectively. Our data also provide information about the behavior of AP molecules during homophilic interactions. First, upon stretching, AP arms did not behave as ideal springs; instead, their stiffness increased gradually (Fig. 2). Second, although the rupture force of a single covalent C–C bond is about 10 nN (14), the strongest measured noncovalent AP-AP binding forces are about 25 times weaker (400 pN). These findings explain why the APs remained intact throughout the AFM experiments and how they allow cell dissociation without being destroyed. Our results indicate that the large cohesive force between two individual sponge adhesion proteoglycans is theoretically able to hold the weight of approximately 1600 cells in physiological solution (15). Thus the integrity of the multicellular sponge organism, with at least 1000 APs per cell (7), may be maintained by the multiplicity of AP-AP interactions.

## REFERENCES AND NOTES

- C. A. Helm, W. Knoll, J. N. Israelachvili, *Proc. Natl. Acad. Sci. U.S.A.* **88**, 8169 (1991); D. E. Leckband, J. N. Israelachvili, F.-J. Schmitt, W. Knoll, *Science* **255**, 1419 (1992).
- G. Binnig, C. F. Quate, C. Gerber, *Phys. Rev. Lett.* **56**, 930 (1986).
- G. U. Lee, D. A. Kidwell, R. C. Colton, *Langmuir* **10**, 354 (1994); E.-L. Florin, V. T. Moy, H. E. Gaub, *Science* **264**, 415 (1994); U. Dammer *et al.*, paper presented at the NATO ASI Workshop, Schluchsee, Germany, 6 to 18 March 1994 (Kluwer, Dordrecht, Netherlands, in press).
- M. Radmacher, M. Fritz, H. G. Hansma, P. K. Hansma, *Science* **265**, 1577 (1994).
- J. T. Finer, R. M. Simmons, J. A. Spudis, *Nature* **368**, 113 (1994).
- T. Humphreys, *Dev. Biol.* **8**, 27 (1963); C. B. Caudwell, P. Henkert, T. Humphreys, *Biochemistry* **12**, 3051 (1973).
- G. N. Misevic, J. Finne, M. M. Burger, *J. Biol. Chem.* **262**, 5870 (1987); G. N. Misevic and M. M. Burger, *ibid.* **268**, 4922 (1993); D. Spillmann *et al.*, *ibid.*, p. 13378.
- J. E. Jumbly, V. Schlup, M. M. Burger, *Biochemistry* **19**, 1038 (1980).
- Silicon nitride cantilevers (0.01 N/m) (10) and atomically flat silicon wafers were made biocompatible by the following procedure: 3 nm of chromium and 30 nm of gold were deposited on the two surfaces by evaporation in high vacuum. They were then immersed in 1 mM 11,11'-dithio-bis-(undecanoic acid *N*-hydroxysuccinimide ester) in dry acetone (P. Wagner, unpublished data), incubated for 12 hours at room temperature, washed in dry acetone, and dried. This procedure led to a self-assembled monolayer of active succinimide groups [A. Ulmann, *An Introduction to Ultrathin Organic Films* (Academic Press, New York, 1991); D. Anselmetti *et al.*, *Europhys. Lett.* **27**, 365 (1994)]. AP molecules purified from *Micrococcina prolifera* marine sponges were covalently attached to these organic monolayers by their amino groups [G. T. Harmanson, A. K. Mallia, P. K. Smith, *Immobilized Affinity Ligand Techniques* (Academic Press, San Diego, 1992)] according to the following procedure: The AP solution was diluted to a final concentration of 0.2 mg/ml in 0.5 M NaCl, 2 mM  $\text{Ca}^{2+}$ , and 20 mM Hepes buffer (pH 7.4) and incubated for 1 hour in a moist chamber at room temperature. The tip and substrate were then rinsed with SWT containing 2 mM  $\text{Ca}^{2+}$  and mounted wet into the fluid chamber of the atomic force microscope (NanoScope III, Digital Instruments, Santa Barbara, CA). The AP-AP interactions were then studied during closely

**Fig. 3.** AFM measurements of AP-AP binding strength. Data were obtained from approximately 1000 approach-and-retract cycles over a period of 6 to 8 hours. Sequential measurements were carried out with the specified cation or mAb in SWT, with exchange of solution after 120 cycles. (A)  $\text{Ca}^{2+}$  and  $\text{Mg}^{2+}$  dependence of the AP-AP adhesion force in SWT. (B)  $\text{Ca}^{2+}$  and  $\text{Mg}^{2+}$  dependence of the AP-AP binding probabilities (11). (C) Effect of antibodies on AP-AP adhesion force. Fab fragments of mAb block 2 or control mAb (both immunoglobulin G2b) were used at 20  $\mu\text{g}/\text{ml}$  in SWT with 10 mM  $\text{Ca}^{2+}$ . Washing of antibodies was done with 5 ml of SWT containing 10 mM  $\text{Ca}^{2+}$  for 1 hour. (D) Aggregation of AP-coated beads, done as described in (7).



- supervised approach-and-retract cycles (10) in SWT containing different concentrations of  $\text{Ca}^{2+}$  and  $\text{Mg}^{2+}$ .
- Approach-and-retract cycles are sometimes called force distance curves or force plots. While the cantilever deflection was permanently monitored, the tip was slowly moved (0.1 Hz) toward the substrate until contact and was then retracted. The hysteresis is a direct measure of the adhesion force. The stiffness of the cantilevers (Park Scientific Instruments, Mountain View, CA) was verified within 30% by taking approach-and-retract cycles on top of three different Si levers that had been individually calibrated by the manufacturer.
  - For steric and statistical reasons, the approach-and-retract cycles did not always result in an adhesion peak. The frequency is a measure of interaction probabilities.
  - D. J. Rice and T. Humphreys, *J. Biol. Chem.* **258**, 6394 (1983).
  - This length assumes that the g200 acidic glycan had the extended structure of a hyaluronate polyanion [W. T. Winter and S. Arnott, *J. Mol. Biol.* **117**, 761 (1977)].
  - A Lennard-Jones (12-6) potential has two free parameters that can be adjusted with respect to the experimental parameters: binding energy (348 kJ/mol) and binding length (0.154 nm). For an individual C-C bond, the gradient of the potential is the negative force and the calculated maximum is the rupture force.
  - The Archimedes force,  $gV(\rho_{\text{cell}} - \rho_{\text{buffer}})$ , equals 0.15 to 0.35 pN, where  $g$  is the acceleration due to gravity (9.81 N/kg),  $V$  is the volume of a cell (for example, a sphere 10  $\mu\text{m}$  in diameter),  $\rho_{\text{cell}}$  is the density of a cell [measured as in C. Gutierrez *et al.*, *J. Immunol. Methods* **29**, 57 (1979)], and  $\rho_{\text{buffer}}$  is the density of seawater (1020  $\text{kg}/\text{m}^3$ ).
  - We selected imaging of physisorbed rather than covalently attached APs because (i) on a nonfunc-

tionized mica substrate the polysaccharide AP arms are also attached to the surface, and (ii) the smoothness of the mica facilitated imaging of the very fine AP arms. For the EM images, the mica was charged by incubation in 3-aminopropyltriethoxysilane (APTS) (Fluka) for 4 min at room temperature. Images are similar to those in S. Humphreys, T. Humphreys, J. Sano, *J. Supramol. Struct.* **7**, 339 (1977).

- We thank D. Hartman, Z. Markovic, and G. De Libero for helpful discussions and critical reading of this manuscript, M. Dreier and M. Hegner for useful comments, E. Paris for technical assistance, and M. Häner for the EM imaging. Supported by Swiss National Science Foundation grants 2000-037496.93 (to H.-J.G.), 3100-037733.93, and 3100-039721.93 (to G.N.M.), and Cancer League Basel grant 5354 (to G.N.M.).

11 October 1994; accepted 20 December 1994

## A Regulatory Role for ARF6 in Receptor-Mediated Endocytosis

Crislyn D'Souza-Schorey, Guangpu Li, Maria I. Colombo, Philip D. Stahl\*

Adenosine diphosphate-ribosylation factor 6 (ARF6), ARF6 mutants, and ARF1 were transiently expressed in Chinese hamster ovary cells, and the effects on receptor-mediated endocytosis were assessed. Overexpressed ARF6 localized to the cell periphery and led to a redistribution of transferrin receptors to the cell surface and a decrease in the rate of uptake of transferrin. Similar results were obtained when a mutant defective in guanosine triphosphate hydrolysis was expressed. Expression of a dominant negative mutant, ARF6(T27N), resulted in an intracellular distribution of transferrin receptors and an inhibition of transferrin recycling to the cell surface. In contrast, overexpression of ARF1 had little or no effect on these parameters of endocytosis.

Intracellular membrane trafficking involves a series of membrane budding and fusion events. These are regulated by specific cytosolic and membrane-associated protein factors, among which are a group of Ras-like small guanosine triphosphatases (GTPases) called adenosine diphosphate (ADP)-ribosylation factors (ARFs), originally identified as cofactors required for the cholera toxin-catalyzed ADP ribosylation of  $\text{G}\alpha_s$  (1). The ARF family consists of 15 structurally related gene products that include 6 ARF proteins and 11 ARF-like proteins (2). The ARF proteins are divided into three classes on the basis of size and amino acid identity. ARFs 1 to 3 (181 amino acids) form class I, ARFs 4 and 5 (180 amino acids) form class II, and ARF6 (175 amino acids) forms class III (3).

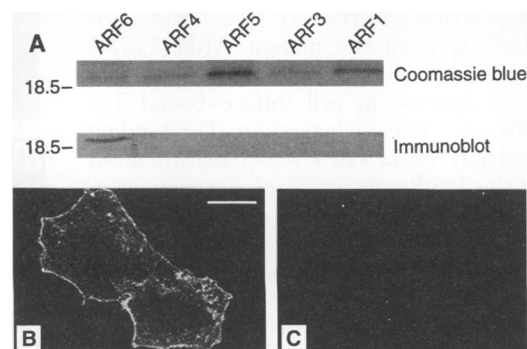
The best characterized ARF protein is ARF1. It is localized to the Golgi apparatus (4) and has a central role in intra-Golgi transport. It is involved in the recruitment of cytosolic coat proteins to Golgi membranes

during the formation of transport vesicles (5). The ARFs are also implicated in endoplasmic reticulum to Golgi transport (6), nuclear vesicle fusion (7), and endosome fusion (8). In these cases, however, the specific ARFs involved and their molecular

mechanisms of action are less clear. Here, we demonstrate that ARF6 is localized to the cell periphery and that overexpression of ARF6 or ARF6 mutants (but not ARF1) causes dramatic alterations in endocytic traffic.

Our studies were carried out in a Chinese hamster ovary cell line that overexpresses the human transferrin receptor (TRVb-1) (9). We transiently expressed ARF6 by using Sindbis virus as an expression vector (10). To monitor the expression of ARF6 and to determine its intracellular distribution, rabbit antiserum to ARF6 was raised against a peptide corresponding to the COOH-terminal region of the protein. This antiserum reacted specifically with ARF6, and no cross reaction was observed with any of the other ARF proteins tested, including ARF1, ARF3, ARF4, and ARF5, as shown by protein immunoblot analysis (Fig. 1). The antibody was used to localize ARF6 by confocal immunofluorescence microscopy in TRVb-1 cells overexpressing ARF6. The overexpressed protein exhibited a peripheral distri-

**Fig. 1.** (A) Specificity of the ARF6 antibody. BL21(DE3) bacteria coexpressing ARF proteins and *N*-myristoyltransferase were grown in 2 ml of Luria broth to an absorbance at 600 nm of 0.8 and were then induced with isopropyl- $\beta$ -D-thiogalactopyranoside for 2 hours. The cell pellet was resuspended in SDS sample buffer, boiled for 5 min, and centrifuged at high speed. Aliquots of the supernatant were run on 12% SDS gels. The SDS gel proteins were visualized by Coomassie blue staining or were transferred to nitrocellulose membranes and blotted with an ARF6 antibody (23). Size markers are indicated on the left in kilodaltons. (B and C) Localization of ARF6 by confocal immunofluorescence microscopy. TRVb-1 cells grown on cover slips were infected with recombinant virus expressing ARF6 (24). At 5 hours after infection, cover slips were fixed with 2% formaldehyde (freshly diluted with PBS) for 15 min, quenched, and permeabilized with PBS containing 0.1 M  $\text{NH}_4\text{Cl}$ , 0.2% gelatin, and 0.05% Triton X-100. Incubation with the affinity-purified ARF6 antibody (B) or immunoglobulin G (IgG) fraction from the preimmune serum (C) was conducted at room temperature for 2 hours. The secondary antibody was a goat antibody to rabbit IgG coupled to fluorescein isothiocyanate (FITC). The cover slips were mounted in 1% propyl gallate and viewed with a Zeiss axiovert microscope and a Bio-Rad confocal scanning imaging system. Bar = 10  $\mu\text{m}$ .



Department of Cell Biology and Physiology, Washington University School of Medicine, 660 South Euclid, Box 8226, St. Louis, MO 63110, USA.

\*To whom correspondence should be addressed.